FOURTEENTH EUROPEAN ROTORCRAFT FORUM

Paper No. 77

HELICOPTER STABILITY AND CONTROL MODELING IMPROVEMENTS AND VERIFICATION ON TWO HELICOPTERS

D. P. SCHRAGE
D. A. PETERS
J. V. R. PRASAD
W. F. STUMPF
CHENGJIAN HE

SCHOOL OF AEROSPACE ENGINEERING
GEORGIA INSTITUTE OF TECHNOLOGY
ATLANTA, GA 30332
U.S.A.

September 20 - 23, 1988
MILANO, ITALY

HELICOPTER STABILITY AND CONTROL MODELING IMPROVEMENTS AND VERIFICATION ON TWO HELICOPTERS

D. P. Schrage, D. A. Peters and J. V. R. Prasad
Professors and Asst. Professor

W. F. Stumpf and Chengjian He
Graduate Students
School of Aerospace Engineering
Georgia Institute of Technology
Atlanta, GA 30332

ABSTRACT

Still unanswered questions in helicopter stability and control mathematical modeling are the degrees of freedom required in linear models and the proper use of techniques for mathematical model verification and updating from flight test. Over the past two years researchers at Georgia Tech's Center of Excellence for Rotary Wing Aircraft Technology (CERWAT) have had a collaborative effort with the Army Aeroflightdynamics Directorate personnel at NASA Ames Research Center aimed at improving helicopter stability and control modeling. This paper presents a summary of the results of this systematic effort to determine the degrees of freedom required in linear models.

LIST OF SYMBOLS

A_o, A_1, B_1	Coning, longitudinal and lateral flapping
C_T, C_L, C_M	Thrust, roll and pitch moment coefficients
$[M]$	Apparent mass matrix
$[L]$	Induced inflow influence coefficient matrix
V	Flow parameter
V_T	Total velocity
α	Rotor disk angle of attack
$\nu_o, \nu_{1s}, \nu_{1c}$	Induced inflow components
μ	Advance ratio
λ	Total inflow
$\xi_o, \xi_{1s,1c}$	Lead-Lag degree of freedoms

1. INTRODUCTION

Central to virtually all aspects of helicopter design and evaluation is an appropriate mathematical model. Most of the recent efforts in this area have concentrated on the development of nonlinear simulation models. Though essential for establishing ground based simulators and for pilot training, these nonlinear models do not give a clear insight into the vehicle characteristics under various flight conditions. Thus, there is a need for the development of linear models of the vehicle about various operating points or trim conditions. These linear models can be used in establishing the stability and control characteristics of the vehicle and they are very useful for a systematic development and design of the vehicle flight control system. In

addition, the linear models are easy to comprehend and they will form the basis for flying qualities evaluation.

The linear models are represented in state variable form as

$$\dot{x} = [A]\ x + [B]\ u$$

The elements of A and B matrices form the stability and control derivatives of the helicopter about the given operating point. There are three different methods available for developing the helicopter linear model about a given operating point (see Figure 1).

The most commonly used method is to obtain the linear model from a global nonlinear simulation model through a numerical perturbation scheme. In this method, using a nonlinear flight simulation model, the helicopter is first trimmed at a given flight condition. From their equilibrium values the states, x, and the controls, u, are perturbed one at a time to obtain the changes in body forces and moments. Then, the stability and control derivatives are obtained as the ratio of change in corresponding force or moment and the perturbation size of the state or control. Though simple and straightforward, the method is very sensitive to the perturbation size which itself may be dependent on the flight condition. In order for successful implementation of the numerical scheme method, it is often necessary to establish first the perturbation sizes that will result in accurate stability and control derivative values at various flight conditions.

The second method is to obtain the stability and control derivatives through analytical differentiation of the force and moment equation. Due to the complexity of the helicopter force and moment equations, analytical differentiation by manual means may become formidable. However, the task involved gets simplified somewhat by the use of symbolic processing programs such as MACSYMA[1]. The advantage of this method is that once an analytical linear model is obtained, it can be used for parametric studies on a routine basis.

The third method that may be used is to obtain the linear model from simulated nonlinear response data through system identification. Using the global nonlinear simulation program, the helicopter is trimmed at a particular flight condition. From this trim condition, the helicopter response data is obtained for wide band excitation such as 3-2-1-1 inputs in the various controls. From the input-output data, linear models are obtained that would best fit the response data. The advantage of this method is that once the methodology is established, the same may be used to obtain linear models from actual flight test data.

With regard to obtaining linear models from actual flight test data a noteworthy effort is being undertaken by the Advisory Group for Aerospace Research and Development (AGARD) Flight Mechanics Panel (FMP). A working group has been formed to improve rotorcraft system identification techniques and make them more appropriate for use in handling qualities evaluation and flight control system design. The working group, designated WG 18, has identified two specific objectives to be accomplished over the initial two year period. The first objective is to identify and evaluate the strengths and weaknesses of different identification approaches, both time and

frequency domain methods. The second objective is to develop guidelines for the application of identification techniques in order to use them more routinely in design and development. Helicopter databases taken on the DFVLR BO-105, RAE SA-330 (Puma), and the MDHC AH-64 (Apache) are being utilized.

For the collaborative effort with NASA Ames a helicopter mathematical model, designated ARMCOP[2], is being used as a generic model to investigate the degrees of freedom required in linear models. ARMCOP was developed at the NASA Ames Research Center and is suitable for piloted simulation of handling qualities and off-line for investigation of helicopter stability and control issues. The ARMCOP mathematical model is a nonlinear, total force and moment model of a single main rotor helicopter. It has ten degrees of freedom: six rigid body, three rotor flapping, and the rotor rotational degree of freedom. The rotor model assumes rigid blades with rotor forces and moments radially integrated and summed around the azimuth. Flapping dynamics are approximated using a tip-path-plane representation. The effect of reverse flow, compressibility, and stall on rotor aerodynamics are disregarded; however it does include a mathematical model of fuselage aerodynamics, stabilizing surface aerodynamics, a simplified tail rotor, and a general description of the stabilizing and control augmentation system.

While ARMCOP has been appropriate for many investigations there are some improvements that can be made which will enhance this model. In addition, ARMCOP serves as an excellent baseline or starting point for investigating the impact of additional degrees of freedom (DOF's). These improvements include adding the lead-lag DOF of the rotor blade, including inflow dynamics into the model, and then including both the flap, lead-lag and dynamic inflow degrees of freedom into the linearized derivative model. Once these changes have been incorporated into the ARMCOP mode, their individual influence can be evaluated by modeling specific helicopters and comparing the influence of specific DOF's and predicted trim and stability with flight test results. The specific helicopters chosen were the UH-60A Black Hawk Helicopter and the BO-105 hingeless rotor helicopter. The remainder of this paper will discuss the modifications made to ARMCOP and provide results on efforts to date.

2. GENERAL DESCRIPTION OF MODEL IMPROVEMENTS

The modifications to the ARMCOP have been mainly involved with the main rotor. First of all, induced inflow dynamics are added to the rotor aerodynamics representation in order to account for the unsteady wake influence on helicopter rotor response. Including additional rotor lead-lag degree of freedom offers another modification approach. Although the lead-lag dynamics are added mainly for examining its role in helicopter stability aspect, its influence on dynamic response has also been investigated.

2.1 Dynamic Inflow Modeling

It is well known that induced inflow variation associated with the changes in rotor thrust and moments can feed back into the blade angle of attack to significantly affect rotor aerodynamics. Moreover, there is a time lag related with the development of the induced inflow due to the so called apparent mass effect which is a measurable unsteady wake influence over the inflow dynamics. Dynamic inflow modeling offers a means of accounting for such low-frequency effects under unsteady or transient conditions.

The dynamic inflow model used for the modification to ARMCOP is the nonlinear model of Pitt and Peters, Ref. [3]. This model is described by a system of first order ordinary differential equations as follows.

$$\left[M \right] \left\{ \begin{array}{c} \dot{\nu}_0 \\ \dot{\nu}_{1s} \\ \dot{\nu}_{1c} \end{array} \right\} + \left[L \right]^{-1} \left\{ \begin{array}{c} \nu_0 \\ \nu_{1s} \\ \nu_{1c} \end{array} \right\} = \left\{ \begin{array}{c} C_T \\ C_L \\ C_M \end{array} \right\} \qquad (1)$$

Where

$$\left[L \right]^{-1} = \frac{1}{C} \left[\begin{array}{ccc} V_T \frac{4sin\alpha}{1+sin\alpha} & 0 & \frac{15\pi}{64} V_T \sqrt{\frac{1-sin\alpha}{1+sin\alpha}} \\ 0 & -[0.5sin\alpha + \frac{1}{4}(\frac{15\pi}{64})^2(1-sin\alpha)] & 0 \\ \frac{15\pi}{64} V \sqrt{\frac{1-sin\alpha}{1+sin\alpha}} & 0 & -0.5V \end{array} \right]$$

$$\left[M \right] = \left[\begin{array}{ccc} \frac{8}{3\pi} & 0 & 0 \\ 0 & -\frac{16}{45\pi} & 0 \\ 0 & 0 & -\frac{16}{45\pi} \end{array} \right]$$

$$V_T = \sqrt{\lambda^2 + \mu^2}$$

$$V = \frac{\mu^2 + \lambda(\lambda + v_0)}{\sqrt{\lambda^2 + \mu^2}}$$

$$C = \frac{2sin\alpha + (\frac{15\pi}{64})^2(1-sin\alpha)}{1+sin\alpha}$$

$$\alpha = tan^{-1}\left|\frac{\lambda}{\mu}\right|$$

To be consistent with the time marching scheme already implemented in ARMCOP, the dynamic inflow equation has also been coded as a two step integration, i.e.,

$$\begin{Bmatrix} \nu_0 \\ \nu_{1s} \\ \nu_{1c} \end{Bmatrix}_{n+1} = \begin{Bmatrix} \nu_0 \\ \nu_{1s} \\ \nu_{1c} \end{Bmatrix}_n + 0.5\Delta t(3 \begin{Bmatrix} \dot{\nu}_0 \\ \dot{\nu}_{1s} \\ \dot{\nu}_{1c} \end{Bmatrix}_n - \begin{Bmatrix} \dot{\nu}_0 \\ \dot{\nu}_{1s} \\ \dot{\nu}_{1c} \end{Bmatrix}_{n-1}) \qquad (2)$$

As seen from the Equation (1), rotor thrust, roll and pitch moments, (i.e., C_T, C_L, and C_M) serve as forcing functions of dynamic inflow. On the other hand, the induced inflow, ν_0, ν_{1s}, and ν_{1c}, will alter the blade angle of attack, and hence change the rotor blade loading which can further affect rotor flapping dynamics and helicopter body response. When the time constants associated with inflow dynamics, rotor flapping, and body dynamics become comparable, these coupling effects can be remarkable on helicopter transient response.

2.2 Lead-Lag Dynamics

As for lead-lag dynamics, a rigid blade with a lag hinge offset is assumed. A root damper is modelled to provide mechanical damping for the blade lead-lag motion.

The equation of lead-lag motion for a rigid blade is reduced from Ref. [4] which deals with a more general elastic blade. The resulting equation includes contributions from body pitch, roll and vertical motions, blade flapping, pitch-flap coupling, blade precone and dynamic inflow. The rotor lead-lag dynamics are described in terms of multi-blade coordinates in an analogous way to tip-path-plane dynamics, i.e.,

$$\xi(t) = \xi_0(t) - \xi_{1s}(t)\sin\psi - \xi_{1c}(t)\cos\psi \qquad (3)$$

These coordinates have certain physical significances. The ξ_{1s} and ξ_{1c} can well define the motion of the center of mass of the rotor system, while ξ_0 can be related with the rotor rotational degree of freedom. To obtain the equations for each of these degrees of freedom, a harmonic balance is carried out with the symbolic processor program MACSYMA. The resulting equations are too lengthy to copy here. The contributions from lead-lag motion to flapping dynamics and rotor forces and moments have also been worked out and added into the modified program.

3. NUMERICAL RESULTS AND DISCUSSIONS

Results and discussions in this section will deal with the influence on the nonlinear simulation model.

3.1 Response with and without Dynamic Inflow

As a demonstration of the dynamic inflow role in helicopter response prediction, time simulations of the transient response have been run with two helicopters. One is the UH60A Black Hawk which has a fully articulated rotor with four blades; and the other is the BO105, a typical hingeless rotor helicopter with four blades. The flight test data for these two helicopters are used for comparison with numerical simulation results with and without inflow dynamics. The simulation runs perform both trim and transient response based on the mathematical model. The time history of the pilot inputs are taken directly from flight test tape. The time step used in the simulation is properly chosen to be 0.015 second in order to capture the dynamic inflow variation.

The first set of results to be examined are the response of the Black Hawk helicopter to a one-inch lateral stick input in hover (Fig. 2 to Fig. 6). In all these figures, the dashed lines are the measurement test data, the triangles are the ARMCOP results with quasi-steady uniform induced inflow with Glauert fore-to-aft gradient, and the circles are results from the modified ARMCOP with dynamic inflow modeling.

Figure 2 shows the helicopter roll response. The initial oscillation in roll rate is due to trim difference between flight test and numerical simulation, and it has no effect on the response after 0.5 second. Immediately after the stick input, it can be seen that the model with dynamic inflow better predicts the build-up of roll rate. Figure 5a gives the cosine component of induced inflow, which describes the fore-to-aft inflow distribution. It behaves quite differently for the two models. The dynamic inflow model has incorporated a time lag and a contribution from pitching moment that account for the better correlation of the roll rate between new model prediction and flight test data. Figure 3 shows the helicopter pitch response. Again, dynamic inflow theory improves the prediction because of the inclusion of lateral distribution of induced inflow with time lag, as shown in Fig. 5b. It is of interest to note that, for the correlation of yaw rate, Fig. 4, the model with dynamic inflow has also done a better job, which is an indirect effect of dynamic inflow through the improvement of prediction of roll and pitch responses. The helicopter response is recorded in body coordinates, while treating aerodynamics in rotor-wind coordinates. A comparison of the blade flapping response data from the two models has shown that the B_1 flapping, i.e., the lateral tilt of the tip-path-plane is affected

significantly by the inclusion of dynamic inflow. This fact accounts for the different roll-rate response from the two models discussed earlier. The lateral tilt of the tip-path-plane response from the two models is given in Fig. 6.

The response of the BO105 helicopter at 40 knots is now presented. In all the figures for BO105 responses, the solid line is for the flight test data and the dashed line is for the theory prediction. Figures 7 to 8 present the response for longitudinal impulse input at 40 knots forward flight. Figure 7 details the results from ARMCOP without inflow dynamics, and Figure 8 with inflow dynamics. Neither theory has done a satisfactory job in correlation. A possible reason is that this is a flight region near transition, and hence the theories may not work well. However, the theory with dynamic inflow does indicate a smaller overshoot in all angular rate responses. It is worthwhile to mention that the simulation with dynamic inflow shows the correct oscillation period in pitch angle, Fig. 8, but the theory without inflow dynamics results in a response just out of phase, Fig. 7. The results from a lateral step input are plotted in Figs. 9 and 10. Due to the fact that inflow dynamics offers an inflow response with a certain time constant, the theory including this effect provides a better roll-rate-response slope after the pilot input. The inflow dynamics also captures the roll rate transient behavior for step collective stick input, as shown in the comparison between Fig. 11 (without dynamic inflow) and Fig. 12 (with dynamic inflow).

The results reveal that the theory with dynamic inflow has a tendency to underestimate steady state responses of both roll and pitch motion, which implies an overestimated first sine-harmonic and an underestimated first cosine-harmonic downwash. Recent development of a new generalized dynamic inflow theory indicates that a linear radial distribution of the first sine and cosine harmonic components of induced inflow is not good enough to model real flowfield in forward flight. In fact, as far as the fore-to-aft distribution is concerned, the responses of higher mode functions, such as r^3 and r^5, are not small, and can still be more than thirty percent as large as the linear one. For the lateral distribution, the r^3 mode is dominant; and, on the outboard blade sections, it has an effect just opposite to that of the linear one. The simple dynamic inflow theory included in this model only picks up a linear distribution for the first harmonic induced inflow, and therefore it may need to be improved in order to give a better prediction in forward flight. Another possible source for the discrepancy between the ARMCOP nonlinear model prediction and flight test data, especially for the pitch rate, can be due to main rotor wake influence on the tail surface, which has been shown to be significant in forward flight with the linear model in ref. 5.

3.2 Response with and without Lead-Lag Dynamics

No remarkable influence of lead-lag dynamics is evident in either the UH-60A or the BO-105 nonlinear simulation responses.

Figures 13 to 16 illustrate the effect of incorporating the lead-lag degree of freedom into ARMCOP. All the results are for the response of Black Hawk helicopter to a half inch longitudinal step input at 60 knots forward flight. Figures 13 and 14 are for rotor tip-path plane response. As indicated in these figures, a small difference exists between trim with and without the

lead-lag degree of freedom. Figures 15 and 16, show the helicopter roll and pitch rate responses where no noticeable effect of adding lead-lag dynamics can be seen. Similar runs have also been performed for BO105 at 40 knots forward flight. Again no remarkable influence of lead-lag dynamics is evident. However, the major effect of lead-lag may be in collective response.

4. LINEARIZED REPRESENTATION OF HELICOPTER DYNAMICS WITH ROTOR DYNAMICS AND DYNAMIC INFLOW

4.1 Addition of Flapping, Lead-Lag and Dynamic Inflow to the Linear Model

In order to investigate the importance of modeling the rotor degrees of freedom for stability and control purposes, the existing linearized model in ARMCOP, which represented only the six rigid body degrees of freedom, was extended to include the flapping, lead-lag and dynamic inflow degrees of freedom. With these additions, the model has 15 degrees of freedom and 23 states. The linear, first order set of differential equations is of the form

$$[E]\{\dot{x}\} = [F]\{x\} + [G]\{\delta\} \tag{4}$$

where

$$\{x\} = \{u_b w_b q_b \theta v_b p_b \phi r_b \dot{\beta}_o \dot{\beta}_{ic} \dot{\beta}_{is} \beta_o \beta_{ic} \beta_{is} \dot{\zeta}_o \dot{\zeta}_{ic} \dot{\zeta}_{is} \zeta_o \zeta_{ic} \zeta_{is} v_o v_{ic} v_{is}\}^T$$

and

$$\{\delta\} = \{\delta_e \ \delta_c \ \delta_a \ \delta_p\}^T$$

All these quantities represent purturbations from trim values.

The elements of the E, F and G matrices are of two types. The first type consist of inertial and gravitational terms obtained analytically from the equations of motion. These express the influence of the body on the rotor degrees of freedom. The flapping degree of freedom terms were taken from the linear flapping equations implemented in ARMCOP's simulation and documented in reference 2. The lead-lag expressions were extracted from the nonlinear lead-lag equations[4]. The non-linear terms were linearized by hand. The dynamic inflow expressions are a linear version of the Pitt-Peters dynamic inflow mode[3].

The contributions of the rotor degrees of freedom to the rigid body forces and moments were expressed as numerical stability derivatives. These consists of partial derivatives of aerodynamic forces and moments with respect to purturbations of {x} and {δ} from trim values. For example,

$$X_u = \frac{\partial X}{\partial u} = \frac{X(u_0 + \Delta u) - X(u_0 - \Delta u)}{2\,\Delta u} \tag{5}$$

The existing six degree of freedom linear model implemented in ARMCOP served as the basis for the rigid body degree of freedom equations. This

model combines analytical expressions with numerical derivatives. The contributions of flapping, lead-lag and dynamic inflow to the rigid body were represented by numerical derivatives. The G matrix is a combination of numerical and analytical terms.

4.2 Reduction of the 15 Degree of Freedom Model to Lower Order Models

The linear, first order equations include the rigid body, flapping, lead-lag and dynamic inflow degrees of freedom. To investigate the importance of each of these, selected degrees of freedom were eliminated. This was done by setting the $\{\dot{x}\}$ terms in the selected equation to zero and then solving for the associated $\{x\}$ values. This $\{x\}$ was then subtracted from the [F] terms. For example, to eliminate the lead-lag degree of freedom from the system matrices E and F, the equations are reduced from

$$\begin{Bmatrix} \dot{x}_{rb} \\ \dot{x}_{fl} \\ \dot{x}_{ll} \\ \dot{x}_{di} \end{Bmatrix} = \begin{bmatrix} F_{11} & F_{12} & F_{13} & F_{14} \\ F_{21} & F_{22} & F_{23} & F_{24} \\ F_{31} & F_{32} & F_{33} & F_{34} \\ F_{41} & F_{42} & F_{43} & F_{44} \end{bmatrix} \begin{Bmatrix} x_{rb} \\ x_{fl} \\ x_{ll} \\ x_{di} \end{Bmatrix} \qquad (6)$$

to

$$\begin{Bmatrix} \dot{x}_{rb} \\ \dot{x}_{fl} \\ \dot{x}_{di} \end{Bmatrix} = \begin{bmatrix} F_{11} & F_{12} & F_{14} \\ F_{21} & F_{22} & F_{24} \\ F_{41} & F_{42} & F_{44} \end{bmatrix} \begin{Bmatrix} x_{rb} \\ x_{fl} \\ x_{di} \end{Bmatrix} - \begin{bmatrix} F_{13} \\ F_{23} \\ F_{43} \end{bmatrix} \left[F_{33} \right]^{-1} \begin{bmatrix} F_{31} & F_{32} & F_{34} \end{bmatrix} \begin{Bmatrix} x_{rb} \\ x_{fl} \\ x_{di} \end{Bmatrix} \qquad (7)$$

Similar expressions result when other degrees of freedom are eliminated.

4.3 Influence of Rotor Dynamics and Dynamic Inflow

Two models were used, the UH-60A as a representative of conventional articulated helicopters, and the hingeless BO105. The Bo105 was modelled as an articulated helicopter with a large effective hinge offset and hub spring. Flight conditions near hover (2 kts) and near cruise (110 kts) were selected to investigate the effect of speed on the linear model.

The effect of the addition of the rotor degrees of freedom can be seen in Figures 18 to 21, which compare the eigenvalues, as degrees of freedom are sequentially added. The effect of increasing model complexity can be seen in the movement of eigenvalues. Enlargements of the region near the origin are also shown to indicate the behavior of the lower roots.

4.3.1 Flapping Degree of Freedom

Addition of the flapping degree of freedom results in six flapping modes and the coupling of body modes with the flap regressing mode. The coupling

can be clearly seen in the large movement of one of the rigid body eigenvalues. On the BO-105 the movement is quite pronounced, as the large hinge offset transmits greater moments to the body. The damping is halved and the period is significantly increased. The coupling with the flapping can also be seen in the eigenvectors for the full 15 degree of freedom system. A detailed analysis of the eigenvectors of these modes indicate that the flap progressing and collective modes are uncoupled, but that the flap regressing and short period modes have coupled together to form two pairs of strongly coupled body-flap modes.

The regressing flapping mode gets coupled to the body mode of the UH-60 differently. Near hover the regressing mode doesn't appear as a complex mode in which flapping dominates but rather as real roots in which cyclic flapping predominates. This occurs because the flapping modes are separated in frequency by Ω, which places the regressing flap mode almost on the real axis. At 110 kts, similar roots are seen, but the eigenvectors show the body to be the greatest contributor. Instead, body flap coupling appears in the high frequency body mode. In addition, the unstable body mode of the Blackhawk moves slightly.

4.3.2 Dynamic Inflow Degree of Freedom

The dynamic inflow modes are very fast and highly damped. Since the dynamic inflow equations are first order, real roots would result from the uncoupled equations. But the inflow couples strongly to flapping, and complex roots result for many flight conditions. The coupling to flapping is noticed from the eigenvector of the complex dynamic inflow mode of the BO-105 near hover. The effect of forward speed on the inflow roots can be seen in figure 22, a plot of the eigenvalues for the BO-105 as velocity is swept from 2 to 110 kts. Note that the vertical scale of this plot has been greatly exaggerated. At 2 kts a pair of complex roots are seen to the left of a real one. As speed is increased, the complex pair moves towards the real axis, becomes real and separates. At the same time the original real root moves to the left causing the center root to move to the left as well. The center root is overtaken by the right one and they become a new complex pair.

Dynamic inflow has a strong effect on the placement of eigenvalues of other modes. Most strongly modified by the addition of dynamic inflow are the high frequency flapping modes, particularly near hover. There, the damping of flap progressing and collective modes is doubled. At higher speeds, the addition of dynamic inflow has a less significant effect as the flapping modes become more damped as flight speed is increased. Both helicopter models behave similarly in this respect.

The slower body-flap mode of the BO-105 near hover has its frequency reduced by the addition of inflow. The other's damping is slightly increased. At high speed the frequency remains unchanged, but the damping is reduced. The real flapping roots for the UH-60, which correspond to the low frequency flapping mode, move toward the origin when inflow is included. Inflow somewhat reduces the damping of the body flap mode for both helicopters. The eigenvectors reveal that the inflow is coupled to other body modes as well, but the damping and frequency of most of these are hardly altered.

4.3.3. Lead-Lag Degree of Freedom

Addition of the lead-lag degree of freedom produces three more complex pairs, corresponding to collective, regressing, and progressing mode. The frequency of these is below that of the flapping roots. As expected in the case of the BO105, the regressing mode is positioned close to collective lead-lag mode. In the case of Blackhawk, this effect is even more pronounced. Here the regressing mode is positioned between the progressing and collective. The progressing and collective modes show almost no coupling with other degrees of freedom, but the regressing is strongly coupled to the body, flapping and dynamic inflow.

The high frequency flapping modes show almost no change due to the addition of lead-lag, but some effect can be seen on the low frequency flapping modes. However, in most cases the movement of the eigenvalues is less than that caused by flapping or dynamic inflow. The movement of the lead-lag regressing, collective and body flap modes over a range of speeds is shown in figure 23 for the BO-105. Initially the lead-lag regressing and body-flap approach each other as speed increases, but then veer off. Lead-lag collective remains almost stationary.

5. SUMMARY AND CONCLUSIONS

A linearized model of helicopter flight dynamics has been developed which includes the flapping, lead-lag and dynamic inflow degrees of freedom. The model is a combination of analytical terms and numerically determined stability derivatives. This model has been used to investigate the importance of the rotor degrees of freedom to stability and control modeling.

These results show that the rotor degrees of freedom can have a significant impact on some of the natural modes in a linear model. The flap and dynamic inflow degrees of freedom show the greatest influence. Flapping exhibits strong coupling to the body, dynamic inflow and to lead-lag to a lesser extent. Dynamic inflow tends to damp the high frequency flapping modes, and reduces the damping on coupled body-flap motion. It also couples to the flapping motion to produce complex roots. Though the lead lag shows less effect than the other degrees of freedom on the natural modes, it can be important in control system design. Work in Reference 5 has indicated that body rate feedback can drive the lead-lag unstable, becoming the limiting factor in the selection of feedback gains. For this reason this degree of freedom should not be neglected in linear models for control system design.

These results have shown essentially similar behavior for most modes of articulated and hingeless rotor helicopters. The exceptions to this are the body-flap and lag regressing modes, which have a different character between the two helicopters.

6. RECOMMENDATIONS

1. In the present study, a linear radial distribution of the first sine and cosine harmonic components of induced inflow has been assumed. The effect of including higher degree spatial distribution of inflow(r^3 and r^5 terms) on the body response characteristics needs further investigation.

2. A numerical perturbation scheme has been used in obtaining the linear models about various equilibrium flight conditions. The accuracy of the results needs to be verified by comparing the results from the present study with results from models derived using other methods such as analytical differentiation of the nonlinear equations of motion, extraction of linear models from response data through system identification, etc.

ACKNOWLEDGEMENTS

This research was supported by the U. S. Army Aeroflightdynamics Directorate under the NASA Ames University Consortium.

7. REFERENCES

[1] Macsyma User's Manual

[2] P. D. Talbot, et al, "A Mathematical Model of a Single Main Rotor Helicopter for Piloted Simulation", NASA TM 84281, September 1982.

[3] D. M. Pitt and D. A. Peters, "Theoretical Prediction of Dynamic-Inflow Derivatives", Vertica, Vol. 5, pp. 21-34, 1981.

[4] Mingsheng Huang, "Coupled Elastic Rotor/Body Vibrations with Inplane Degree of Freedom", Ph.D. Thesis, Georgia Institute of Technology, May 1987.

[5] Zhao, Xin and Curtiss, H. C., "A Linearized Model of Helicopter Dynamics Including Correlation with Flight Test", Proceedings of the Second International Conference on Rotorcraft Basic Research, University of Maryland, College Park, MD, Feb. 1988.

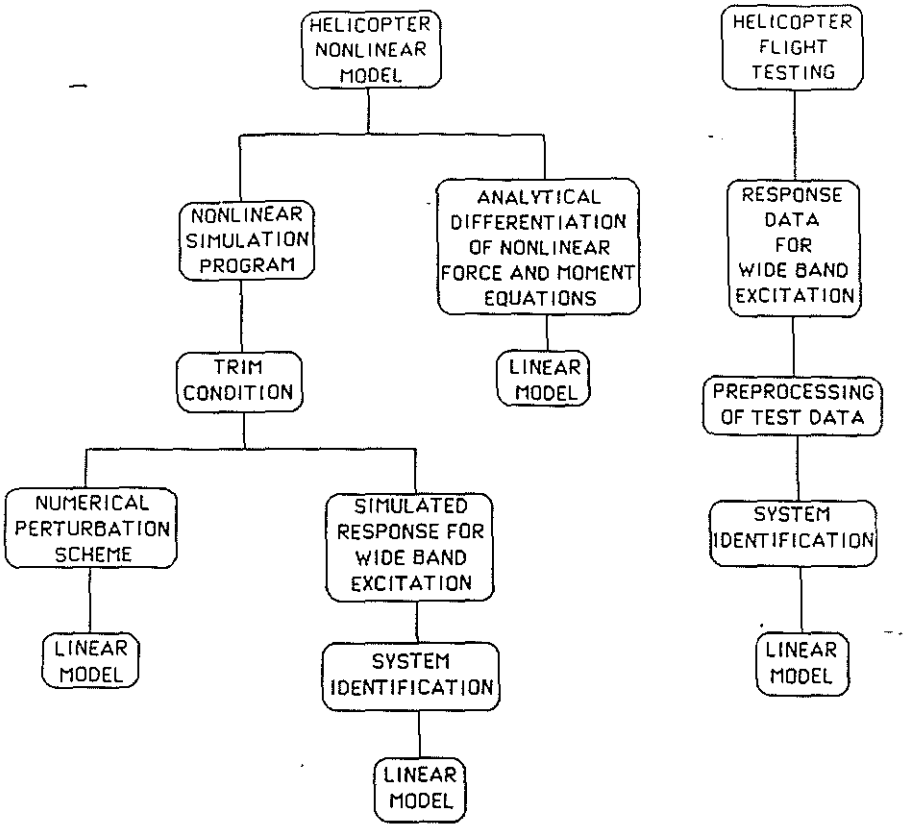

Figure 1. Helicopter Linear Handling Qualities Model Development.

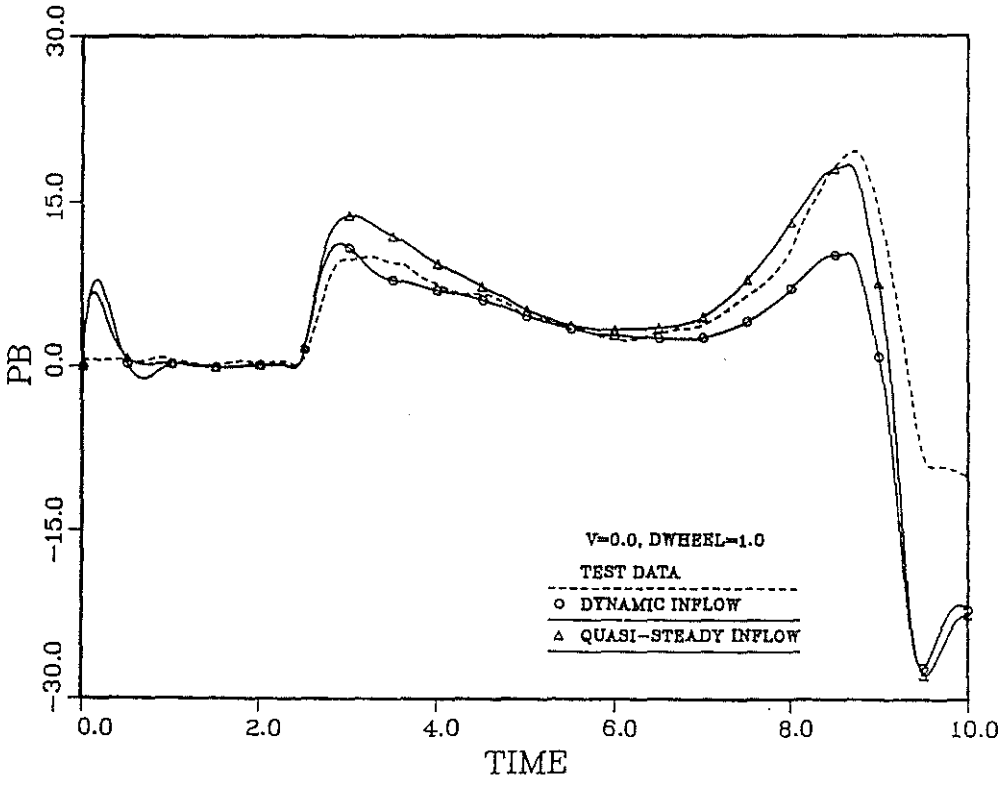

Figure 2. Body Roll Rate Response to 1 inch Lateral Stick Input.

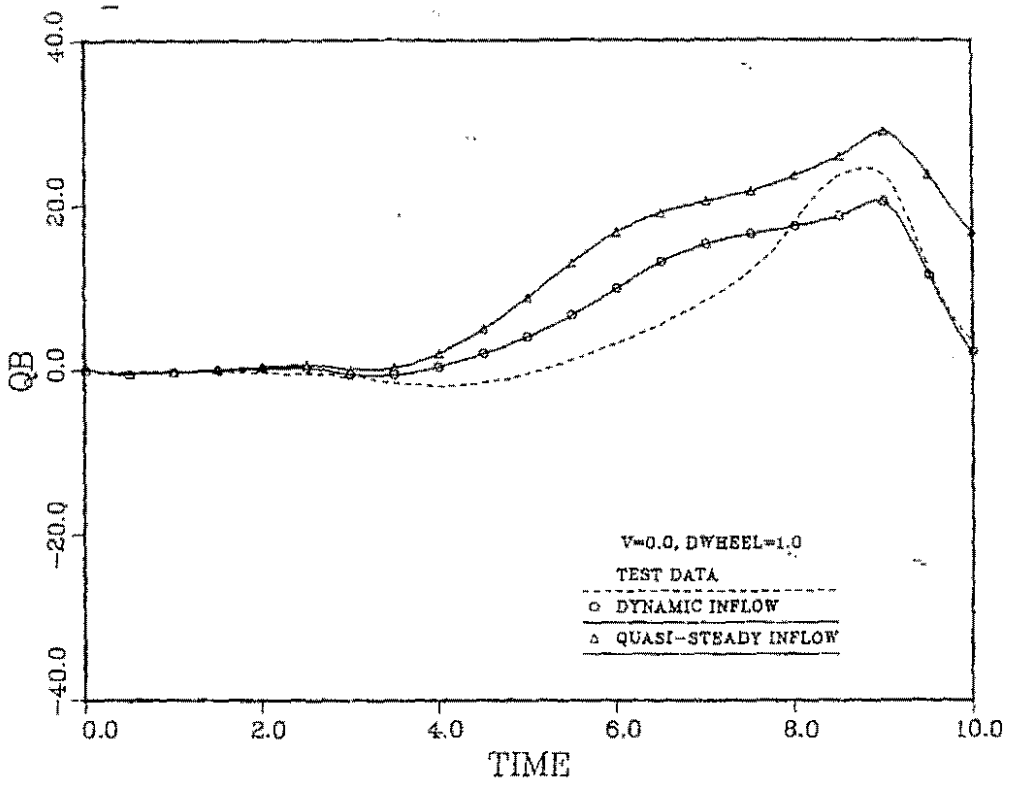

Figure 3. Body Pitch Rate Response to 1 inch Lateral Stick Input.

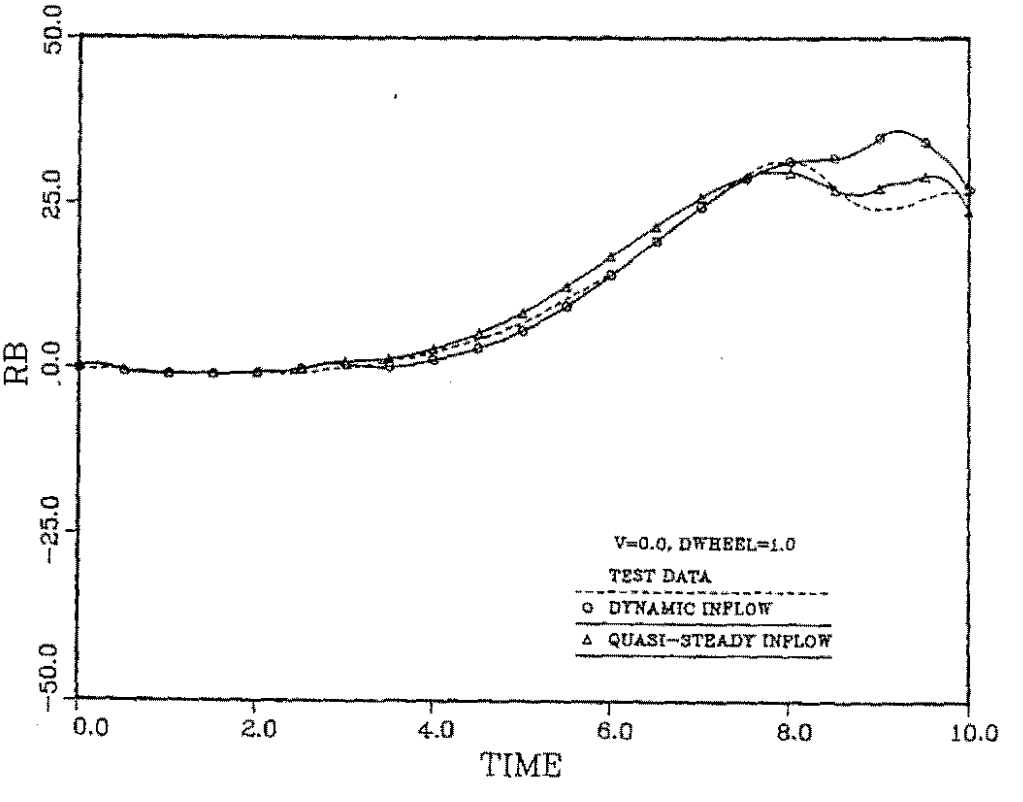

Figure 4. Body Yaw Rate Response to 1 inch Lateral Stick Input.

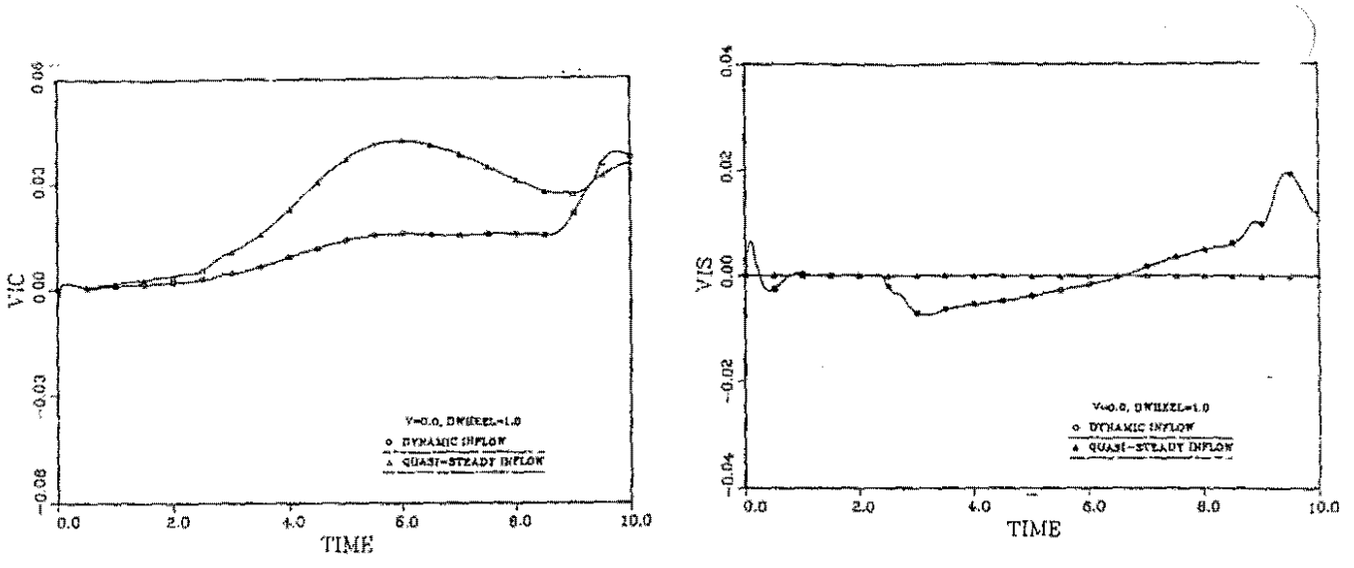

Figure 5. Longitudinal and Lateral Variation of Inflow with Time for 1 inch Lateral Stick Input.

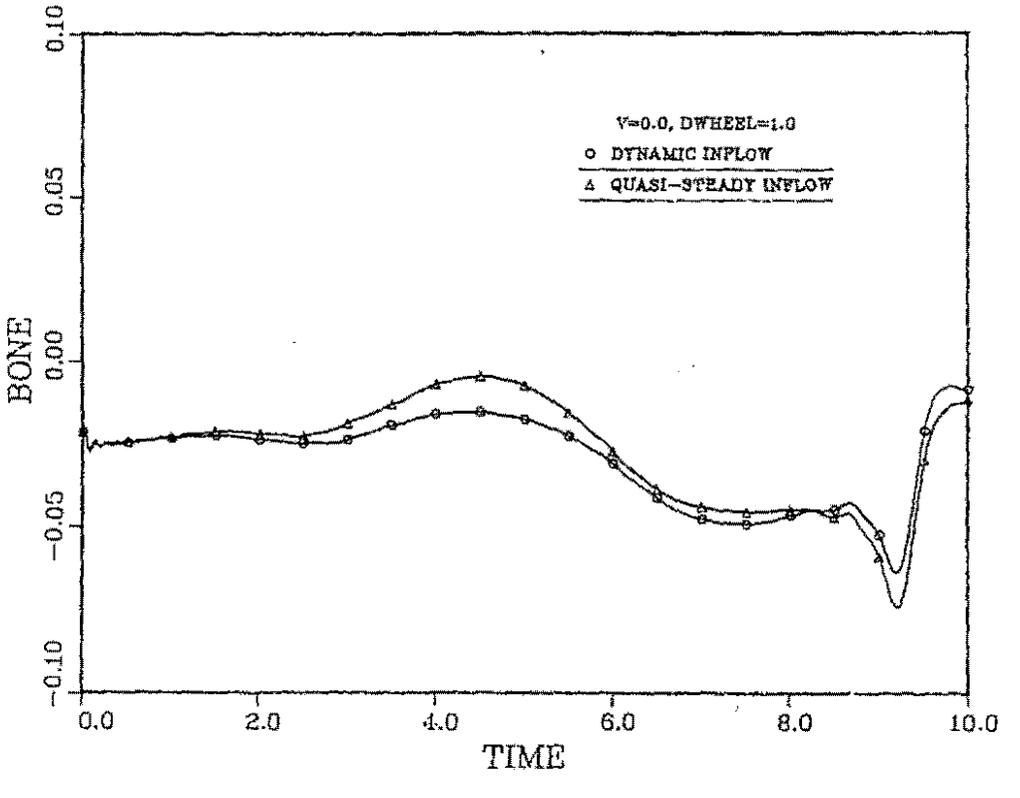

Figure 6. Lateral Tilt of the Tip-Path-Plane Variation with Time for 1 inch Lateral Stick Input.

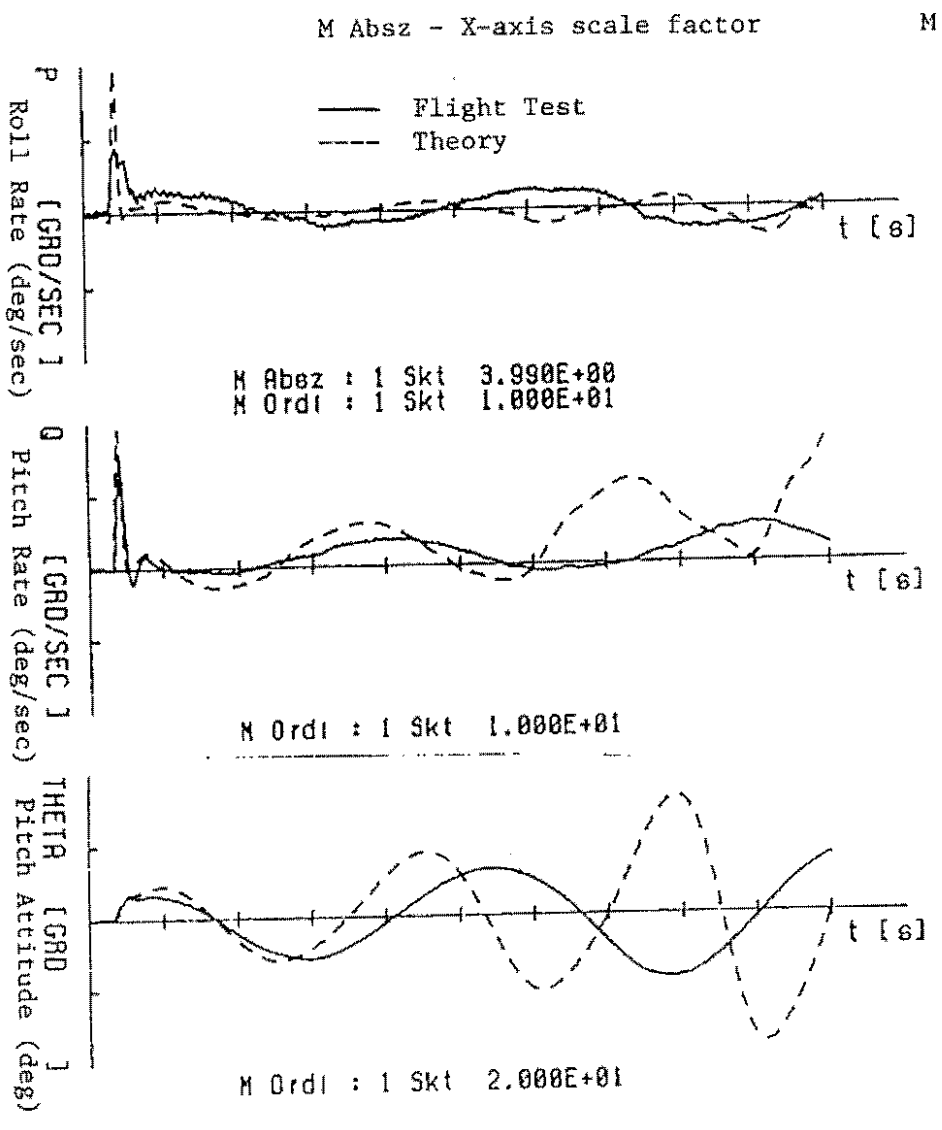

Figure 7. Longitudinal Impulse Input Response without Dynamic Inflow.

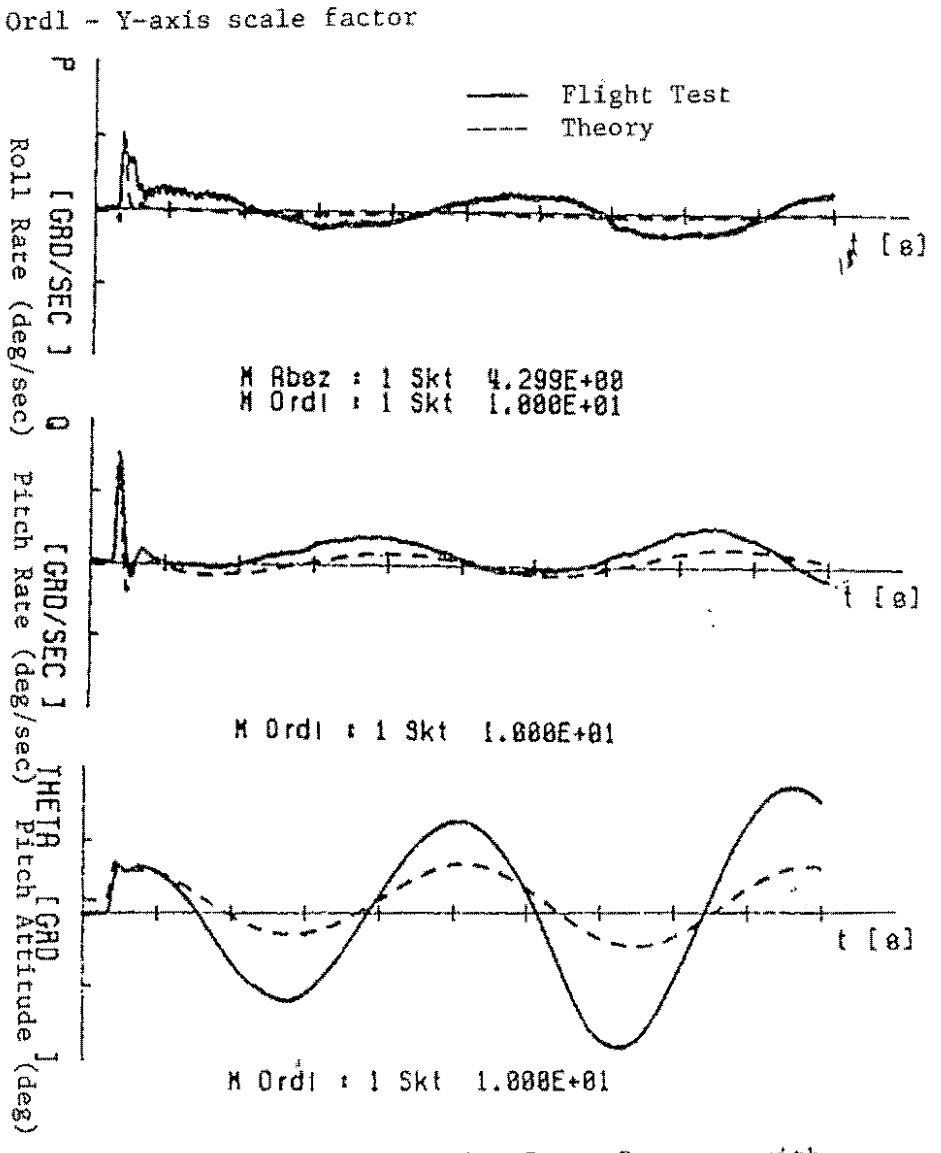

Figure 8. Longitudinal Impulse Input Response with Dynamic Inflow.

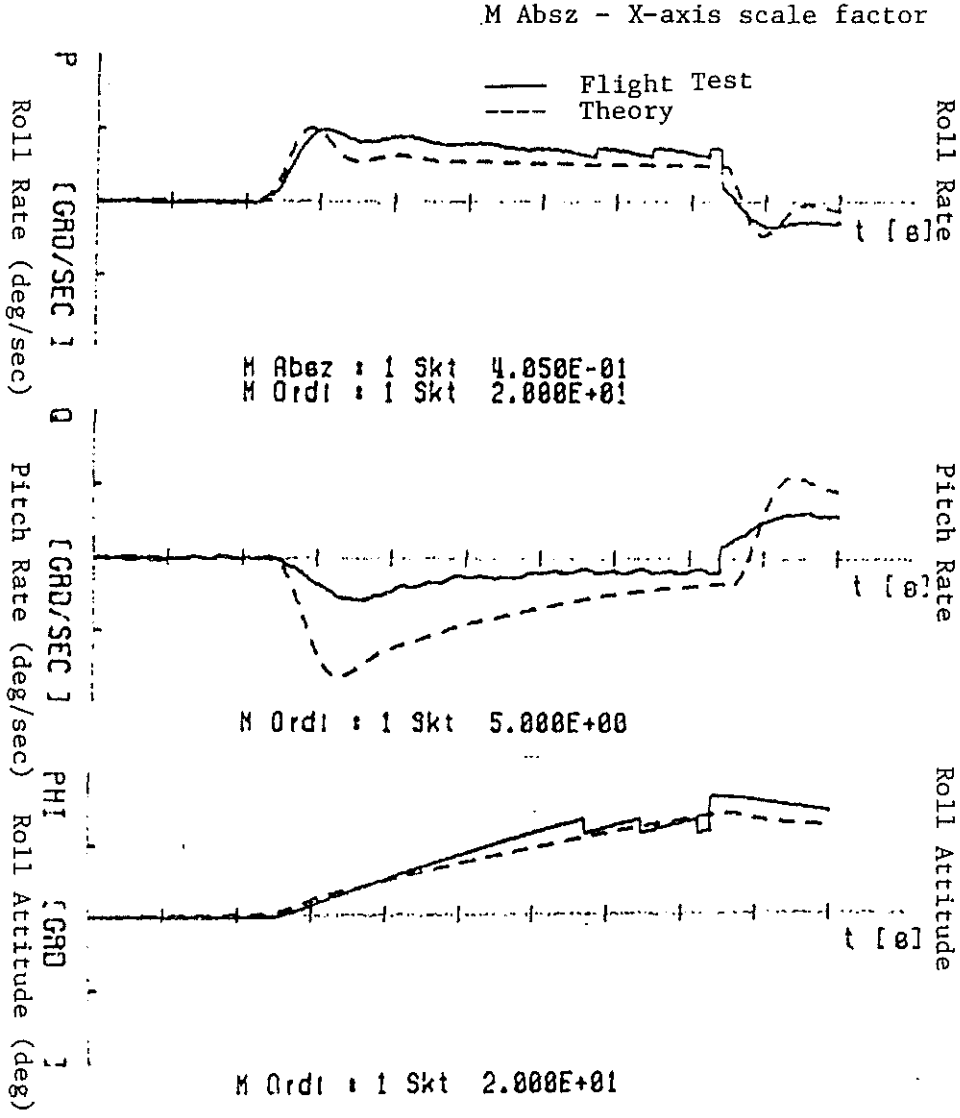

Figure 9. Lateral Stick Input Response without Dynamic Inflow.

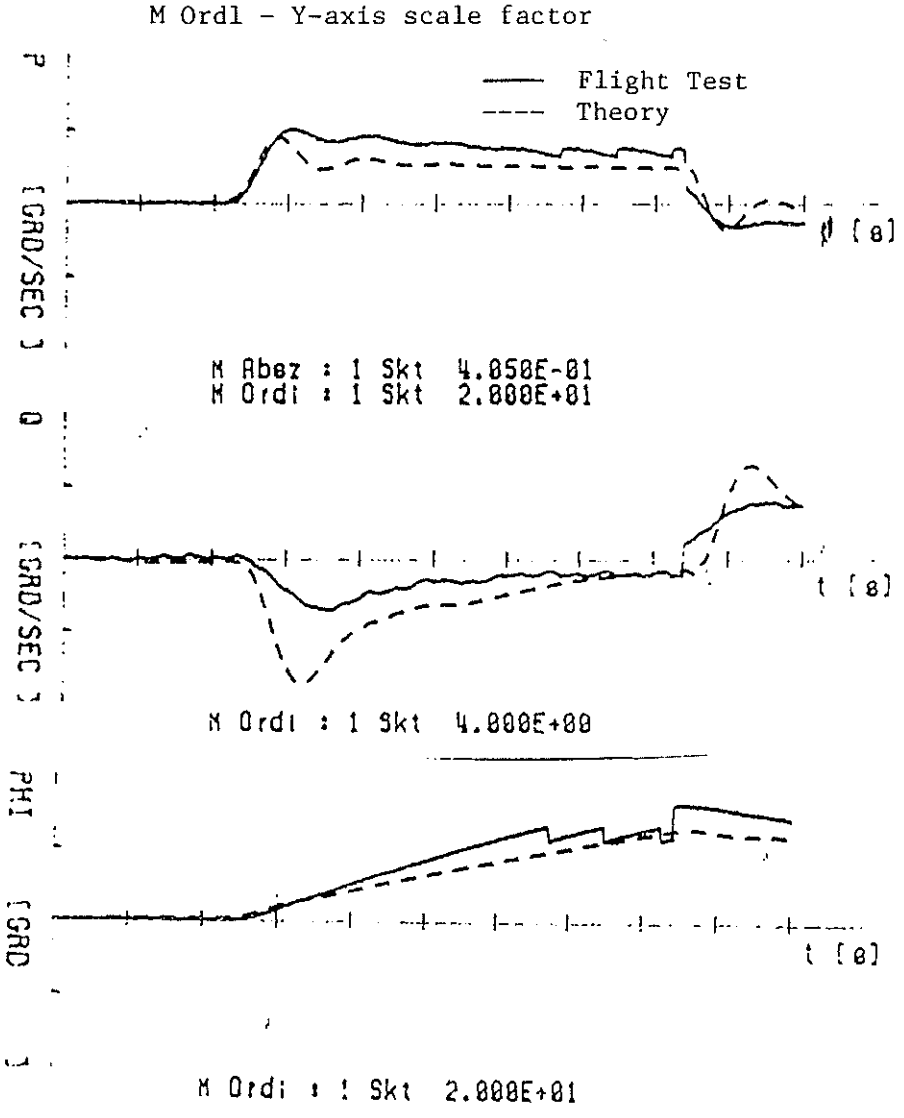

Figure 10. Lateral Stick Input Response with Dynamic Inflow.

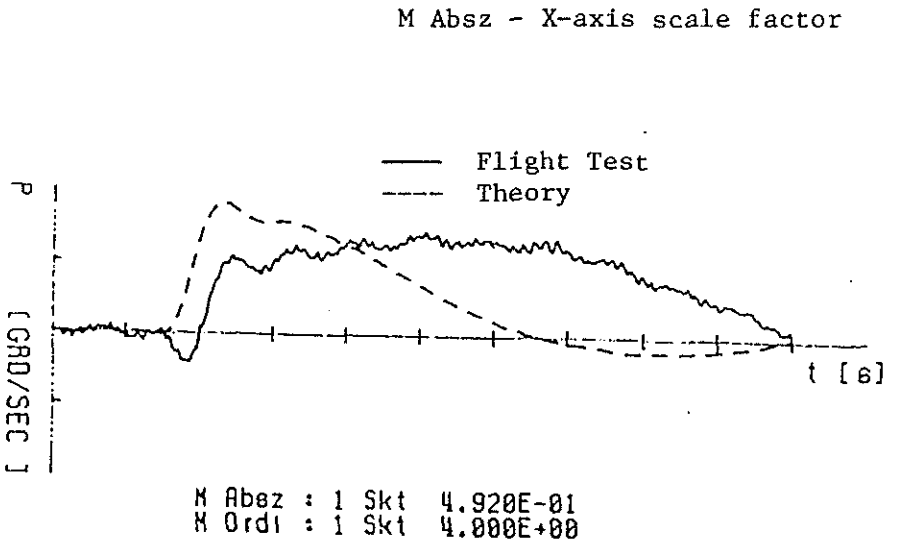

Figure 11. Body Roll Rate Response to a Step Collective Input without Dynamic Inflow.

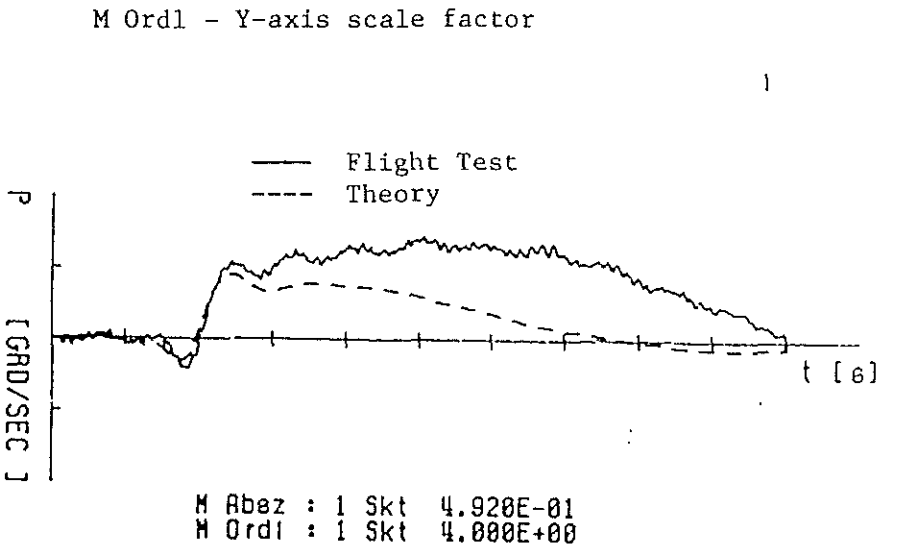

Figure 12. Body Roll Rate Response to a Step Collective Input with Dynamic Inflow.

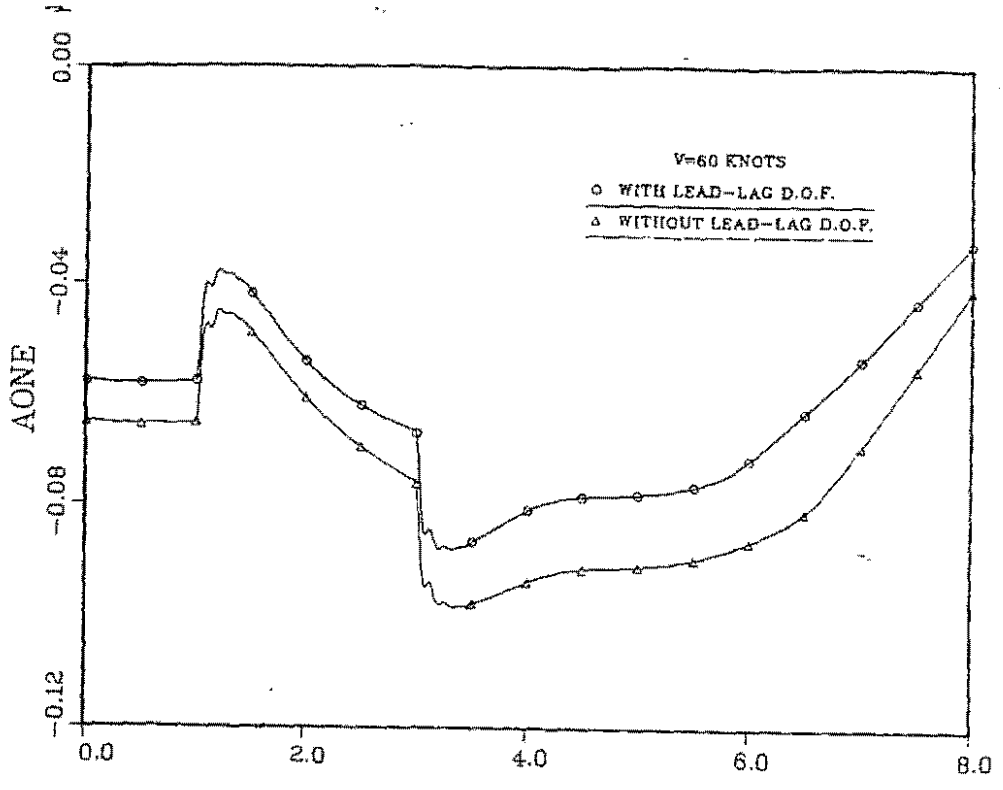

Figure 13. Longitudinal Tilt of Tip-Path-Plane for a half inch Longitudinal Stick Input.

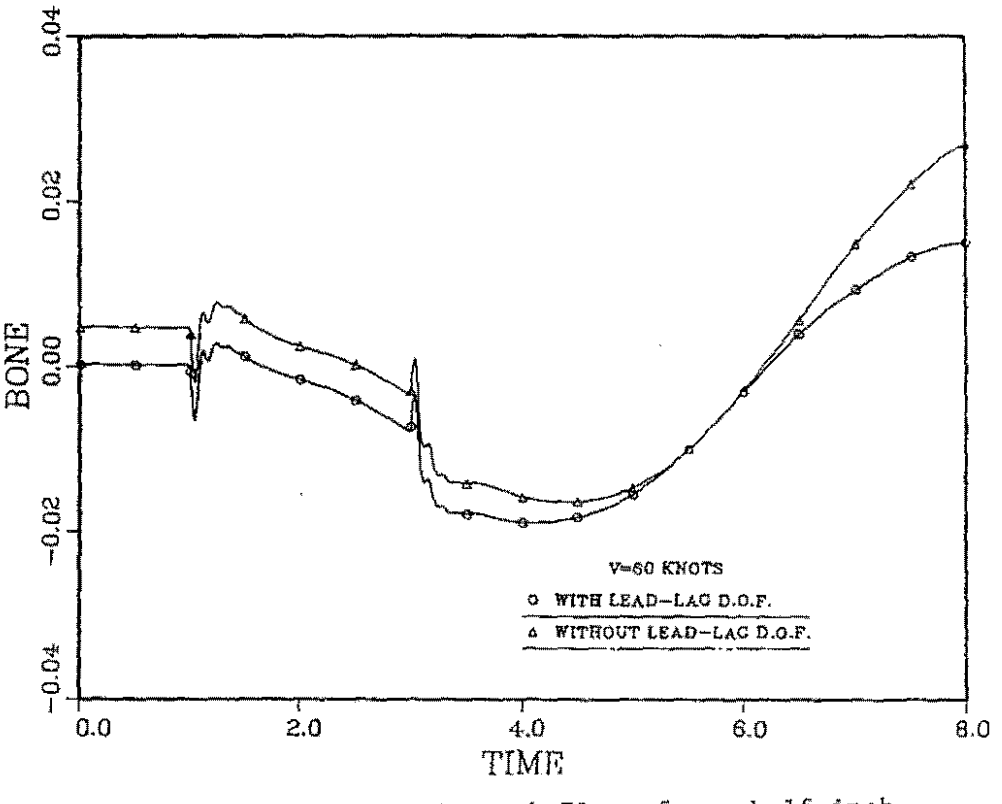

Figure 14. Lateral Tilt of Tip-Path-Plane for a half inch Longitudinal Stick Input.

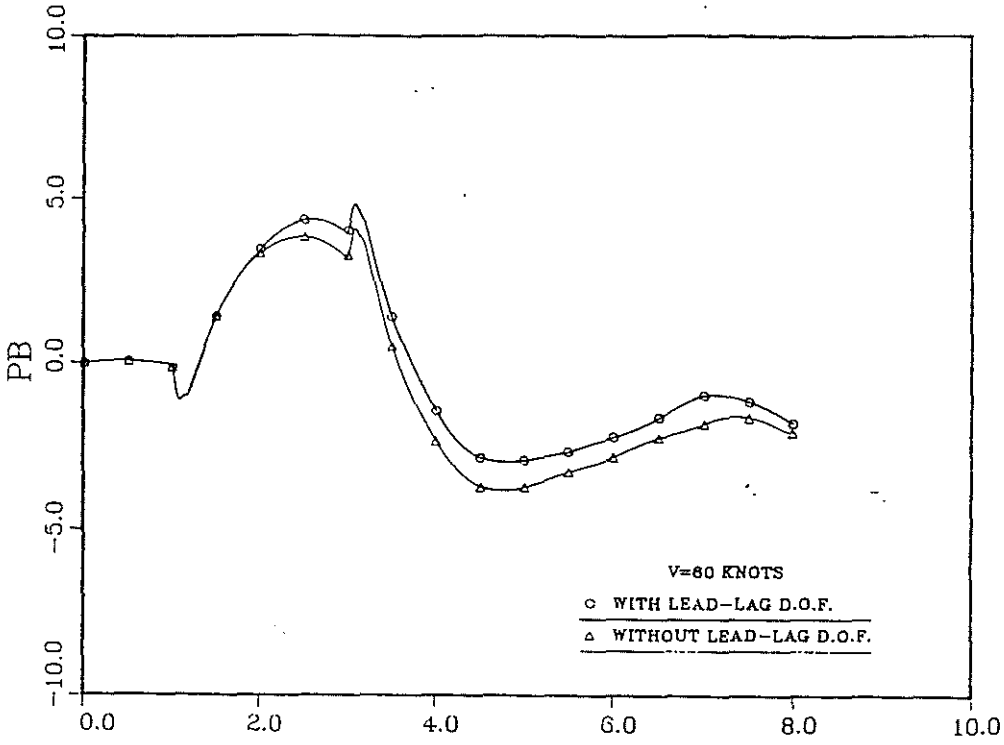

Figure 15. Body Roll Rate Response to a half inch Longitudinal Stick Input.

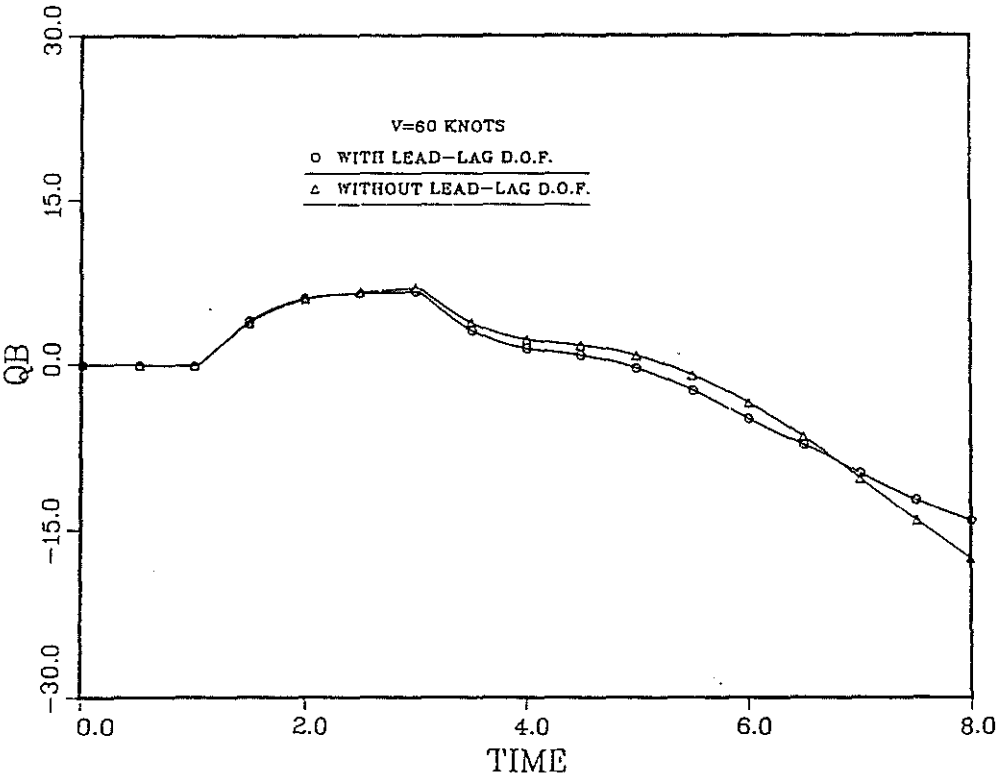

Figure 16. Body Pitch Rate Response to a half inch Longitudinal Stick Input.

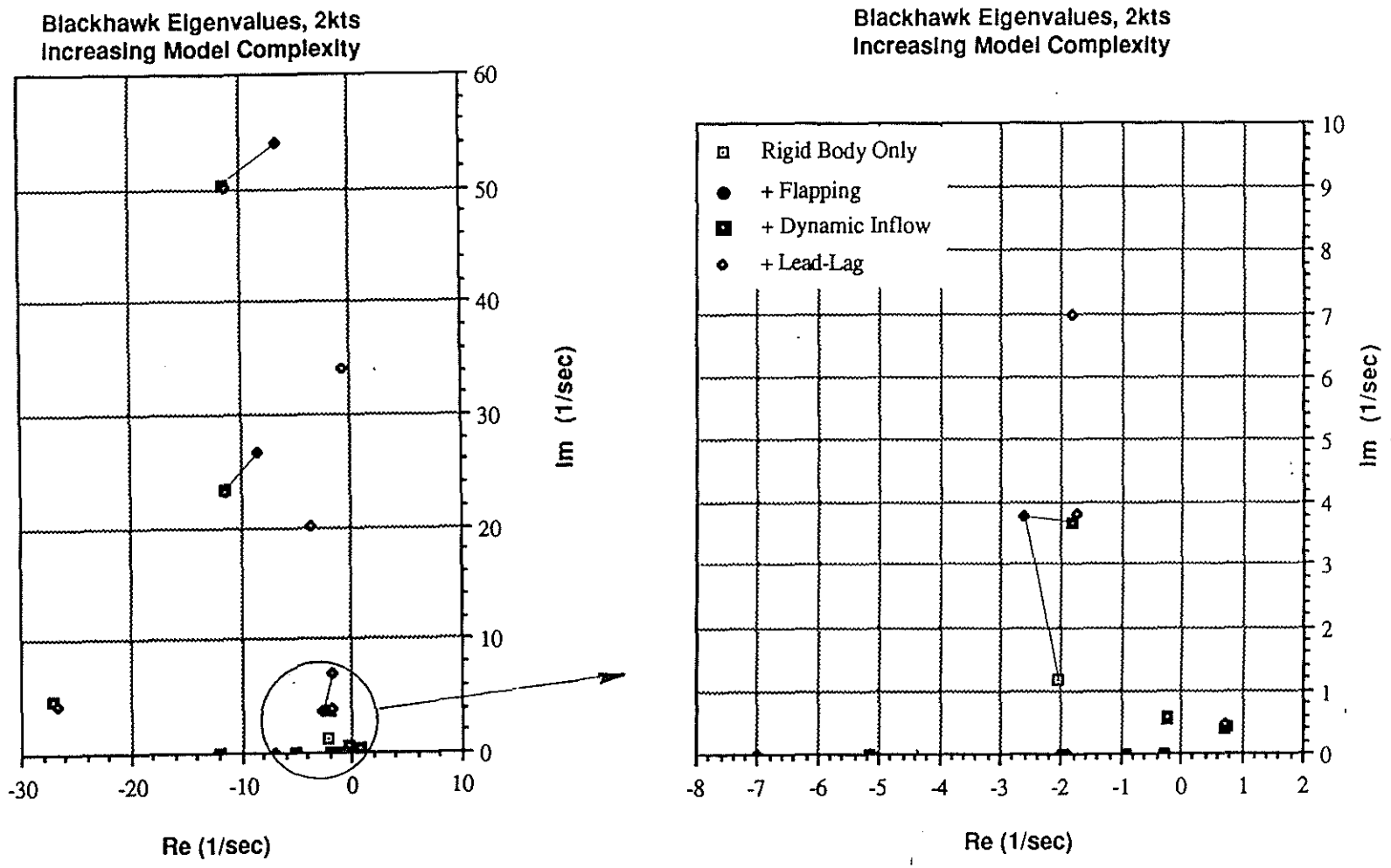
Blackhawk Eigenvalues, 2kts
Increasing Model Complexity
Im (1/sec)
Re (1/sec)
60
50
40
30
20
10
0
-30
-20
-10
0
10
Blackhawk Eigenvalues, 2kts
Increasing Model Complexity
Rigid Body Only
+ Flapping
+ Dynamic Inflow
+ Lead-Lag
Im (1/sec)
Re (1/sec)
10
9
8
7
6
5
4
3
2
1
0
-8
-7
-6
-5
-4
-3
-2
-1
0
1
2

Figure 18

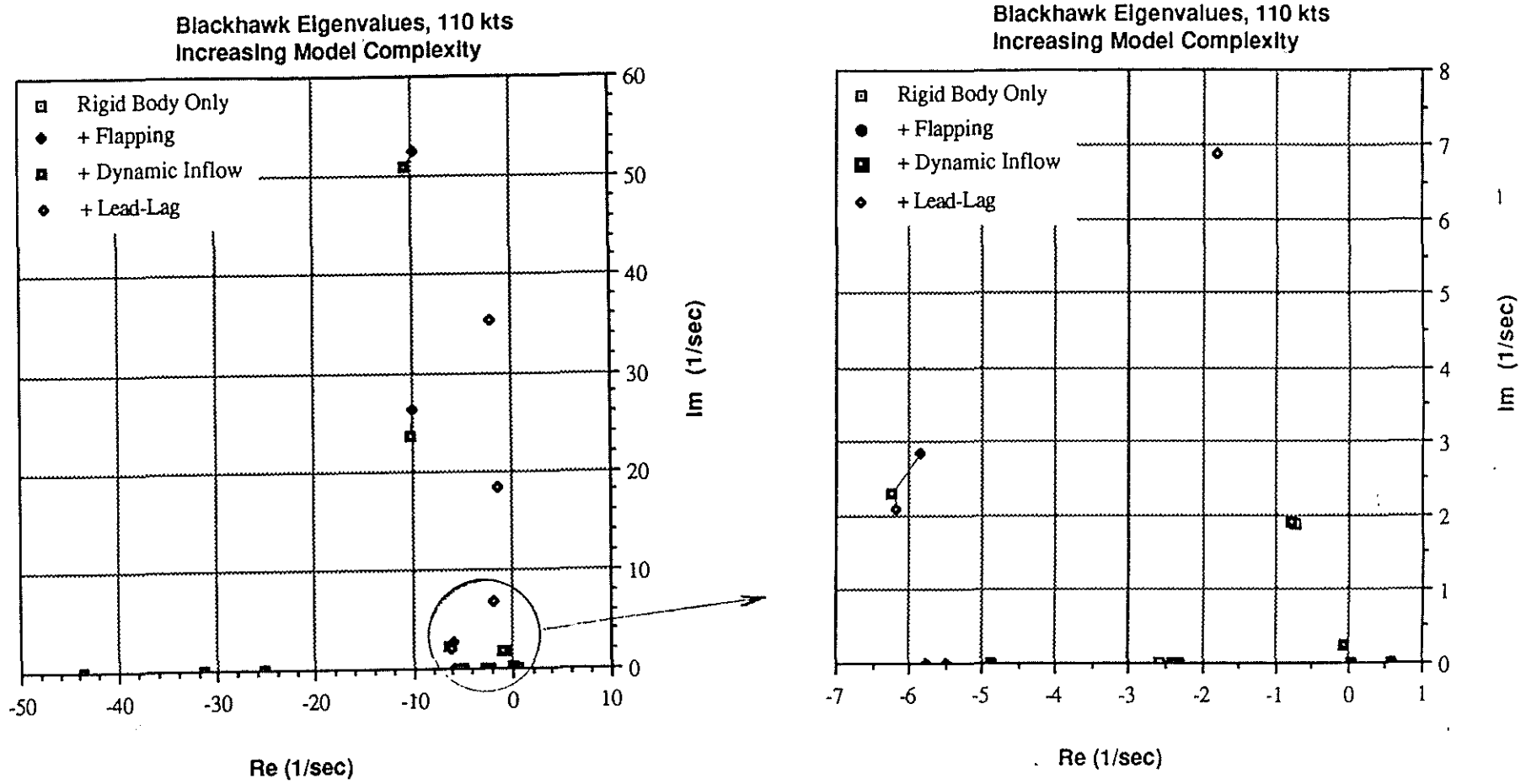
Blackhawk Eigenvalues, 110 kts
Increasing Model Complexity
Rigid Body Only
+ Flapping
+ Dynamic Inflow
+ Lead-Lag
Im (1/sec)
Re (1/sec)
-50
-40
-30
-20
-10
0
10
60
50
40
30
20
10
0
Blackhawk Eigenvalues, 110 kts
Increasing Model Complexity
Rigid Body Only
+ Flapping
+ Dynamic Inflow
+ Lead-Lag
Im (1/sec)
Re (1/sec)
-7
-6
-5
-4
-3
-2
-1
0
1
8
7
6
5
4
3
2
1
0

Figure 19

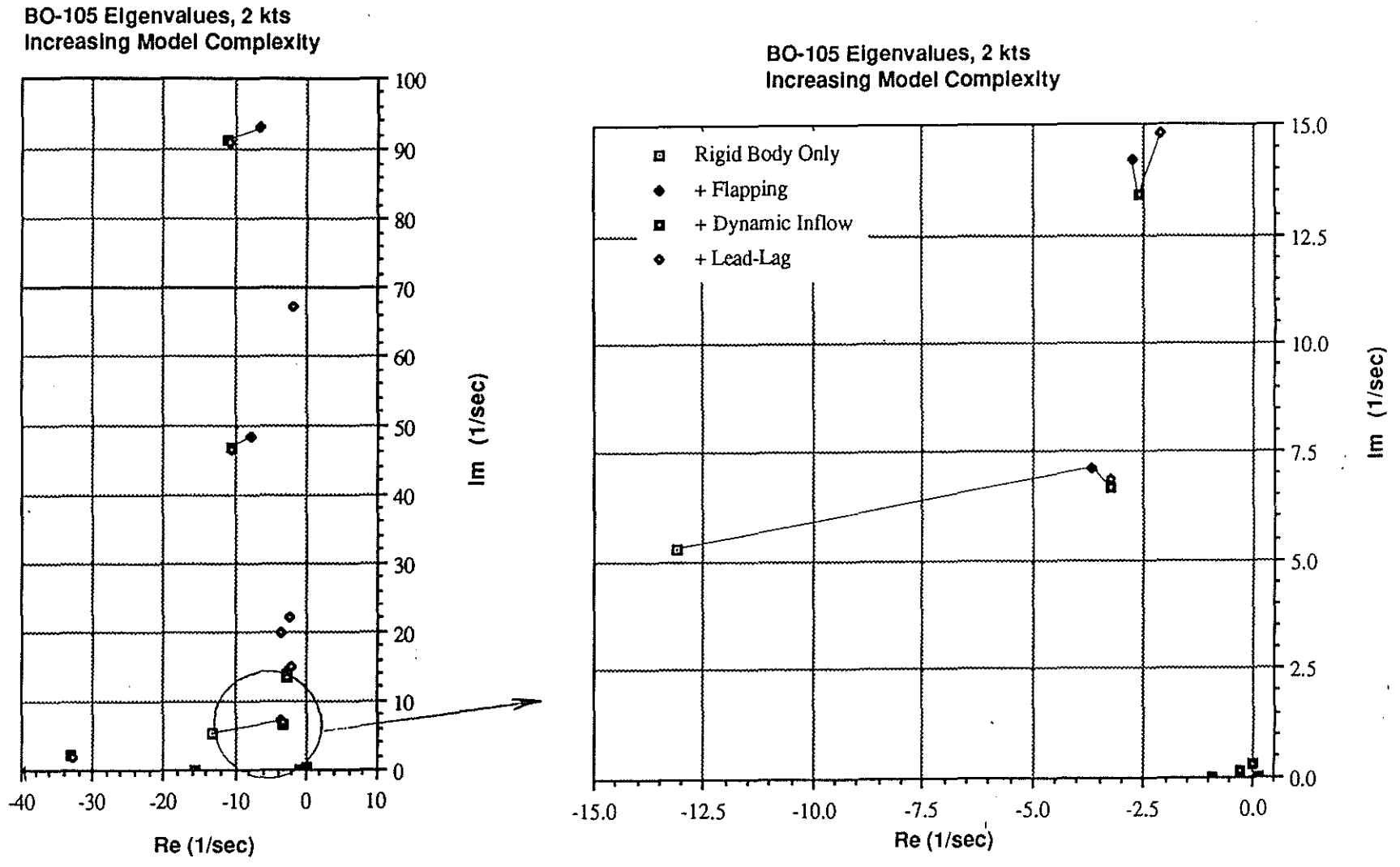
BO-105 Eigenvalues, 2 kts
Increasing Model Complexity
Im (1/sec)
Re (1/sec)
-40
-30
-20
-10
0
10
0
10
20
30
40
50
60
70
80
90
100
BO-105 Eigenvalues, 2 kts
Increasing Model Complexity
Rigid Body Only
+ Flapping
+ Dynamic Inflow
+ Lead-Lag
Im (1/sec)
Re (1/sec)
-15.0
-12.5
-10.0
-7.5
-5.0
-2.5
0.0
0.0
2.5
5.0
7.5
10.0
12.5
15.0

Figure 20

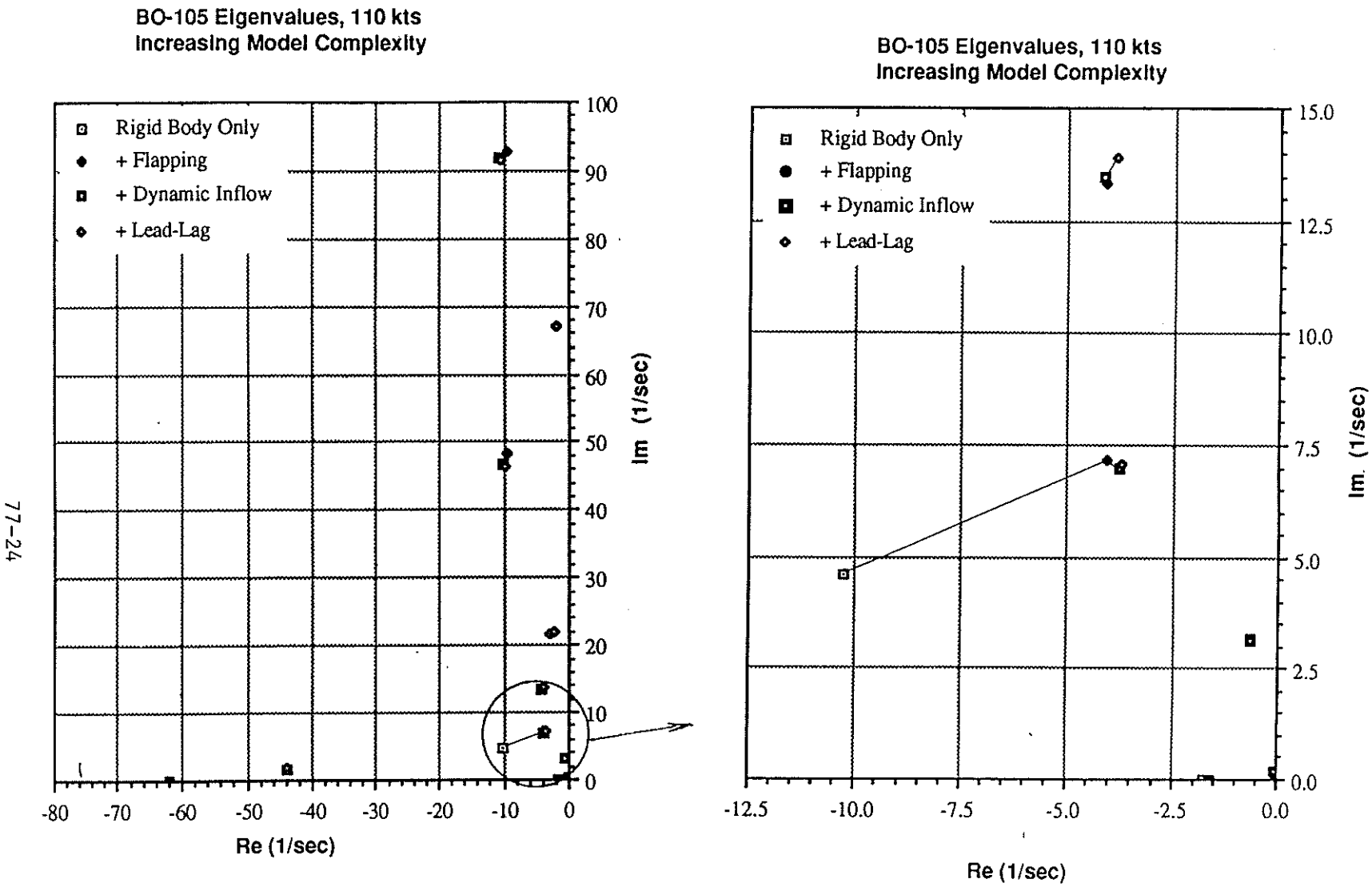
BO-105 Eigenvalues, 110 kts
Increasing Model Complexity
Rigid Body Only
+ Flapping
+ Dynamic Inflow
+ Lead-Lag
Im (1/sec)
Re (1/sec)
-80
-70
-60
-50
-40
-30
-20
-10
0
100
90
80
70
60
50
40
30
20
10
0
BO-105 Eigenvalues, 110 kts
Increasing Model Complexity
Rigid Body Only
+ Flapping
+ Dynamic Inflow
+ Lead-Lag
Im. (1/sec)
Re (1/sec)
-12.5
-10.0
-7.5
-5.0
-2.5
0.0
15.0
12.5
10.0
7.5
5.0
2.5
0.0

Figure 21

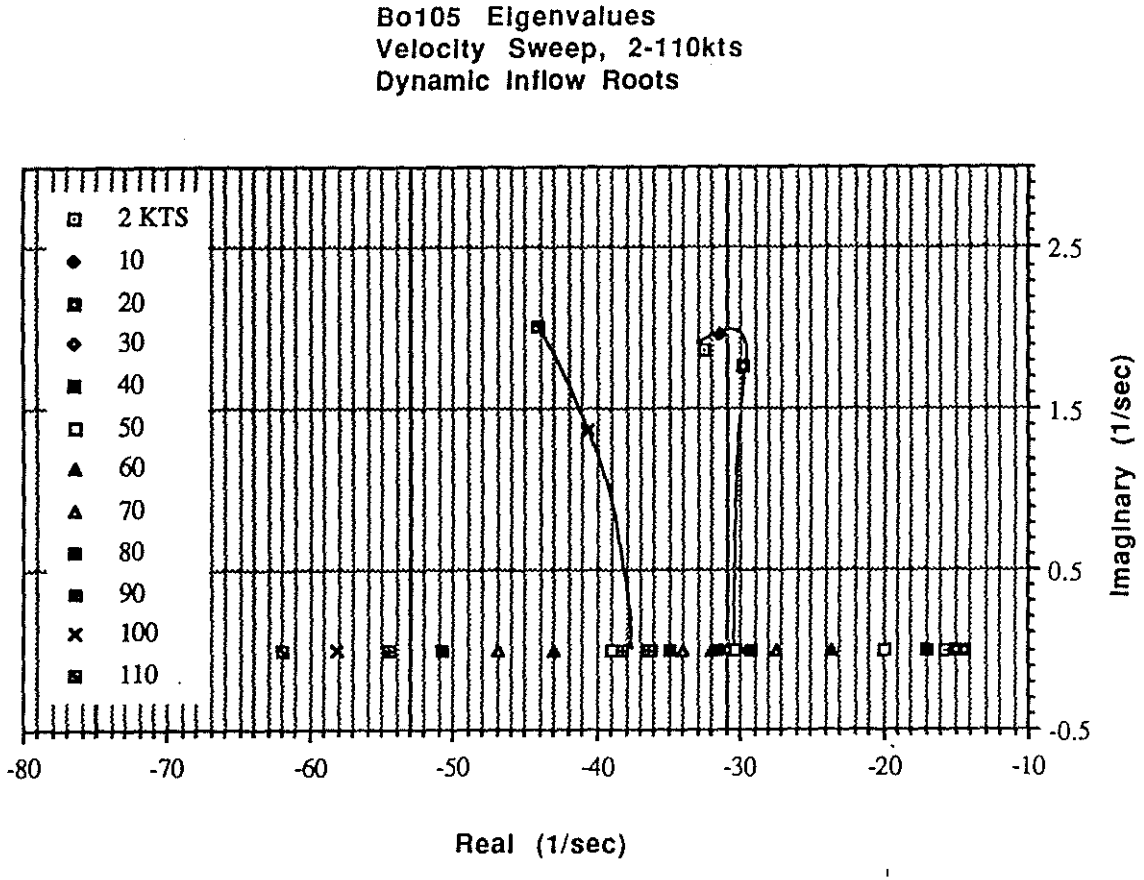

Figure 22. Movement of Dynamic Inflow Roots for Increasing Speed.

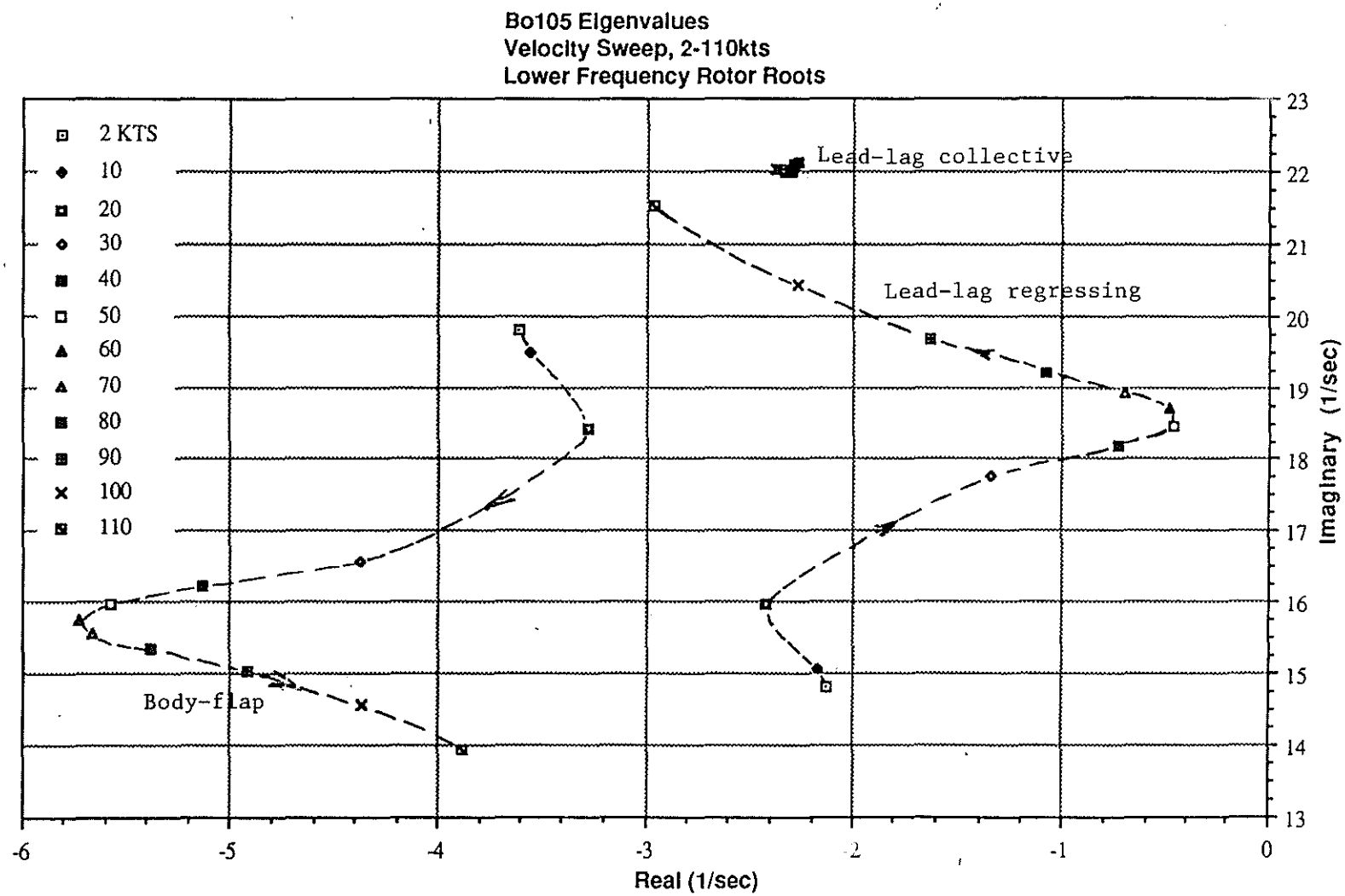

Figure 23. Movement of Low Frequency Rotor Roots for Increasing Speed.